ACCOUNTS of chemical research

Article

pubs.acs.org/accounts

Silica Coated Upconversion Nanoparticles: A Versatile Platform for the Development of Efficient Theranostics

Jia-Nan Liu, Wen-Bo Bu,* and Jian-Lin Shi*

State Key Laboratory of High Performance Ceramics and Superfine Microstructures, Shanghai Institute of Ceramics, Chinese Academy of Sciences, Shanghai 200050, P.R. China

CONSPECTUS: Next generation theranostic devices will rely on the smart integration of different functional moieties into one system. These individual chemical elements will have a variety of desired chemical and physical properties and will need to behave in a multifunctional manner. Researchers have used upconversion nanoparticles (UCNPs) as a basis for superior imaging probes to locate cancerous lesions. The features of these nanoparticles, such as large anti-Stokes shifts, sharp emission bands, long-lived luminescence, and high resistance to photobleaching, have produced versatile probes. One way to improve these probes is to add a layer of dense or mesoporous silica to the outer surface of UCNPs (UCNP@SiO_2). These modified UCNPs are chemically stable and much less cytotoxic than the original UCNPs. In addition, their surface can be easily modified to introduce various functional groups (e.g., $-NH_2$, −COOH, −SH) via silanization, which facilitates conjugations with various biological molecules for multimodal imaging or synergetic therapeutics. This versatility makes UCNP@SiO_2 particles excellent platforms for the construction of efficient theranostics.

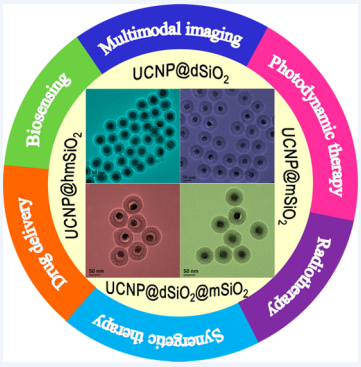

In this Account, we provide a comprehensive summary of recent progress in the development of UCNP@SiO_2 nanocomposites for theranostics in the hope of speeding their translation into the clinic. We first discuss the major design principles and protocols for engineering various nanocomposites based on UCNP@SiO_2 structures including those coated with dense silica, mesoporous silica, or hollow mesoporous silica. Next we summarize several representative efforts that probe the relaxivity mechanisms of these nanostructures as a way to optimize magnetic resonance sensitivity, multimode cancer imaging, near-infrared light-triggered chemotherapy, photodynamic therapy, and synergetic therapy (the combination of radiotherapy with chemotherapy, thermotherapy, or photodynamic therapy) using UCNP@SiO_2-based theranostics.

By rational integration of a wide range of features that convey multiple functions (such as imaging and therapy) into the structure or onto the surfaces of UCNP@SiO_2, the constructed theranostics show promise for multimodal cancer imaging, biosensing, and effective cancer therapy. Finally, we discuss the limitations of UCNP@SiO_2 nanostructures, the difficulties in the design of smart theranostics, and their potential role in clinical cancer research.

1. INTRODUCTION

Recently, upconversion nanoparticles (UCNPs) have attracted considerable attention due to their unique features in converting near-infrared light (NIR) to visible or ultraviolet (UV) light efficiently through an upconversion process.[1] Such upconverted luminescence (UCL) imaging is expected to be the next-generation photoluminescence imaging technique for the detection of cancerous lesions because UCNPs provide many uncommon opportunities in biomedical applications, such as low background autofluorescence from biomolecules, deep photon penetration in tissues, minimal photodamage to living organisms, and high sensitivity.[2] More interestingly, by doping with functional ions such as Gd^{3+}, UCNPs can be readily applied as excellent dual-mode imaging contrast agents, which show a great probability to improve the quality of imaging and thus provide reliable and accurate detection of cancerous lesions.[3] Besides their multiple imaging capabilities, UCNPs have also been widely used in theranostics in which disease diagnosis and therapy are combined and performed on a single nanoplatform.[4] On the basis of these distinctive advantages, recent years have witnessed rapid progress in the research and development of UCNPs for biomedical applications.

In the past decades, diverse routes have been developed for the synthesis of uniform UCNPs.[5] Typically, monodisperse UCNPs of highly uniform size and morphology were synthesized in high-boiling organic solvents such as octadecene. In this synthesis, oleic acid was usually employed as a primary surfactant to modulate the crystal growth by coordinating to the nanoparticle surface. As a result, a subsequent surface hydrophilic modification is usually necessary to provide both a stable aqueous colloidal dispersion and the ability to conjugate biomolecules and other ligands on the UCNP surface before they can be employed in theranostics applications.

In this regard, a large variety of surface modification methods have been developed to convert hydrophobic UCNPs into hydrophilic ones, including chemical modification of the hydrophilic ligand or addition of an extra hydrophilic layer on the UCNPs' surface.[6] Among various methods, the growth

Received: February 15, 2015
Published: June 9, 2015

DOI: 10.1021/acs.accounts.5b00078
Acc. Chem. Res. 2015, 48, 1797−1805

of a silica shell on UCNPs (UCNP@SiO_2) have attracted great interest since they exhibit low cytotoxicity and their chemically active surface can be easily modified to introduce various functional groups (e.g., −COOH, $-NH_2$, −SH, etc.) via silanization, which can satisfy various needs of conjugating biological molecules or functional nanoparticles. Moreover, the large surface area and pore volume of mesoporous silica ensure facile adsorption as well as high loading of various therapeutic materials. Clever combinations of UCNP@SiO_2 nanocomposites with different kinds of functional moieties will enable the development of multifunctional nanomedical platforms for biosensing, multimodal bioimaging, drug delivery, photodynamic therapy (PDT), and synergetic therapy. Hence, the integration of UCNPs and silica make these systems one of the most investigated nanocomposite materials. Therefore, it will be of great significance to introduce the latest progress in this field to the chemical community.

This Account provides an overview of UCNP@SiO_2, including their chemical synthesis strategies, modification and functionalization approaches, and their theranostics applications. We aim to elucidate the general concepts and structure−property relationship of UCNP@SiO_2 and then to provide useful insights into the strategies of achieving a set of desired chemical properties using the UCNP@SiO_2 nanoplatform for practical applications in the future. We hope to stimulate new ideas and inspire continuous endeavors in this emerging research area.

2. SYNTHESIS OF UCNP/SILICA CORE−SHELL STRUCTURES

Silica shells can be in either dense or mesoporous forms. In the following sections, the rational design and synthesis of UCNP@SiO_2 nanomaterials, including both dense and mesoporous silica shells will be highlighted. It is worth mentioning that gold, quantum dots, and superparamagnetic iron oxide nanoparticles can also be embedded into silica shells using the following methods.

2.1. Dense Silica Coating

Dense silica ($dSiO_2$) coating is a versatile strategy to modify the surface of UCNPs. Typically, there are two routes to coat $dSiO_2$ onto UCNPs: one is sol−gel nanochemistry in a reverse micelle nanoreactor[7] to coat $dSiO_2$ onto UCNPs with hydrophobic capping ligands; the other is the Stöber method[8] to make $dSiO_2$ coating provided that the UCNPs' surfaces have already been modified to be hydrophilic.

The reverse micelle method is applied for coating a uniform layer of $dSiO_2$ on oleate- or oleylamine-capped UCNPs (Figure 1a). This method involves the formation of a nanoconfined hydrophilic cavity, which acts as a "nanoreactor", stabilized by a surfactant (e.g., Igepal CO-520) in the organic phase (e.g., cyclohexane). After addition of tetraethyl orthosilicate (TEOS) to the solution, the $dSiO_2$ shell will grow on the surface of UCNPs via ammonia-catalyzed polymerization of TEOS. To ensure the stability of the microemulsion, the final silica shell thickness can be precisely controlled only in the range of 20 to 100 nm by tuning the amount of the added TEOS.

The Stöber method prevails in silica chemistry. This method can be easily applied in the synthesis of UCNP@$dSiO_2$ by mixing hydrophilic UCNPs with water and ammonia to form a homogeneous solution. A uniform $dSiO_2$ shell can be formed around the UCNP via the hydrolysis and condensation of TEOS around the UCNP "seeds". Hence, the precise control of surfactant content essential for creating stable micelles in reverse micelle method is unnecessary in this Stöber approach, thereby facilitating the elaborate manipulation of reactant concentrations to accurately tune the silica shell thickness from 1 nm to 2 μm. For example, Li and Zhang reported the coating of a very uniform $dSiO_2$ shell onto polyvinylpyrrolidone (PVP)-stabilized UCNPs with the controlled $dSiO_2$ thickness of 1−3 nm.[9]

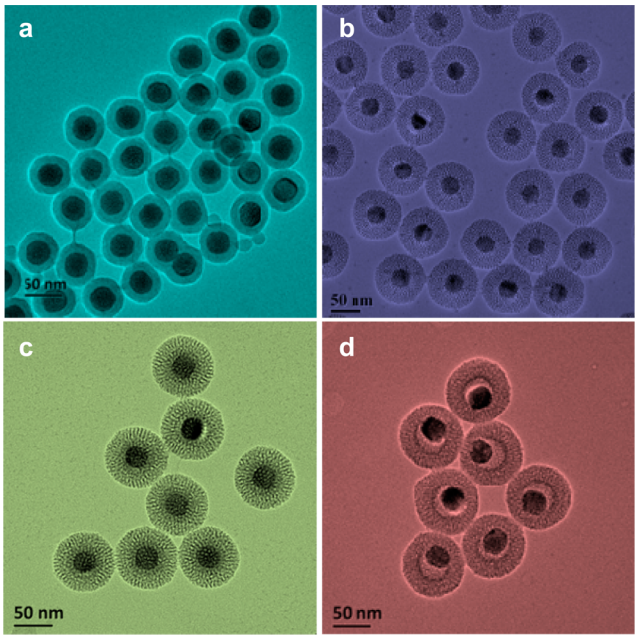

Figure 1. Transmission electron microscopy (TEM) images of various UCNP@SiO_2 nanostructures, including UCNP@$dSiO_2$ (a), UCNP@$mSiO_2$ (b), UCNP@$dSiO_2$@$mSiO_2$ (c), and UCNP@$hmSiO_2$ (d).

2.2. Mesoporous Silica Coating

In general, there are two routes to synthesize the nanocomposites of UCNP@$mSiO_2$. The first is to coat $mSiO_2$ layer directly on the surface of UCNPs in one step; while the second is to coat $mSiO_2$ layers on the surface of UCNP@$dSiO_2$ to form a UCNP@$dSiO_2$@$mSiO_2$ core@shell@shell structure.

Our group reported the direct fabrication of the $mSiO_2$ layer on the hydrophobic surface of UCNPs using temperature-controlled ultrasonication treatment (Figure 1b).[10] In this process, cetyltrimethylammonium bromide (CTAB) serves as both surfactant for transforming hydrophobic UCNPs to hydrophilic ones and organic template for the formation of the mesoporous shell. During the $mSiO_2$ shell coating process, the ultrasonic energy input can effectively prevent the aggregation of nanoparticles at the controlled temperature of 25 °C, which facilitated the formation of monodisperse core−shell nanostructures with single UCNP cores being uniformly coated by $mSiO_2$ shells.

Notably, $mSiO_2$ shells can also be readily coated on UCNP@$dSiO_2$. Typically, an ordered $mSiO_2$ shell with a thickness of 10−100 nm can be uniformly coated around UCNP@$dSiO_2$ nanoparticles by using octadecyltrimethoxysilane (C_{18}TMS) as a mesopore template.[11,12] One drawback of this method is the uncontrolled aggregation of the final nanoparticles during high-temperature treatment (550 °C, 6 h), which seems to be the only known way to remove C_{18}TMS from the silica network. To solve this problem, we used hexadecyltrimethylammonium chloride (CTAC) as template when coating $mSiO_2$ shells.[13]

DOI: 10.1021/acs.accounts.5b00078
Acc. Chem. Res. 2015, 48, 1797−1805

Subsequent extraction of the CTAC using ion exchange (e.g., sodium chloride) yielded a patterned $mSiO_2$ shell (Figure 1c). Compared with direct $mSiO_2$ coating, the incorporation of a $dSiO_2$ interlayer results in improved chemical stability along with tunable separation between the UCNPs core and surface tethered components.

2.3. Hollow Mesoporous Silica Coating

Recently, rattle-structured UCNP@$hmSiO_2$ nanomaterials, which compose of UCNP core, $mSiO_2$ shell and large voids in between the core and the shell, have attracted widespread attention because their high surface to volume ratio and large pore volume are highly desirable for many potential applications.

Etching, or partial dissolution of the interior of nanoparticles, is a widely used approach to synthesize $hmSiO_2$ nanomaterials. Typically, this method involves the growth of two layers of $dSiO_2$ on a hydrophobic UCNP, and the second shell growth is usually accomplished by a water-phase Stöber method. Subsequently, a surface-protected hot water etching process (using PVP as a surface protector) at 95 °C can etch away the first $dSiO_2$ shell by breaking the internal Si−O−Si bonds and in the meantime generate mesopores in the second silica shell, yielding a "yolk" nanostructure with $mSiO_2$ shell. By adjustment of the etching duration, it was possible to obtain a series of intermediate structures with different cavity sizes. To generate bigger pores in the outer silica shell, the mesoporous second silica layer, instead of $dSiO_2$ layer, can be coated before etching (Figure 1d).[13]

3. APPLICATIONS IN IMAGING, BIOSENSING, DRUG DELIVERY, AND SYNERGETIC THERAPY

3.1. Relaxivity Mechanism Probing and MR Sensitivity Optimization

Gadolinium-doped UCNPs (Gd-UCNPs) have been widely documented as both UCL and T_1-weighted magnetic resonance (T_1-MR) imaging agents.[14] Understanding of the relaxivity mechanism of Gd-UCNPs as affected by surface modification is of great significance in guiding MR sensitivity optimization. With this in mind, the origins of the longitudinal (r_1) relaxivity in the situation of various surface modifications were investigated using models of dense and mesoporous silica coated Gd-UCNPs.[15] According to the classical Solomon−Bloembergen−Morgan theory for predicting the efficiency of MRI contrast agents, the overall r_1-relaxivity involves two contributions: inner-sphere relaxivity (r_1^{IS}, bonding of water molecules directly to Gd^{3+} ions) and outer-sphere relaxivity (r_1^{OS}, no water to Gd^{3+} ion bonding is needed).[16] Typically, three critical parameters (q, the number of water molecules coordinated by a single Gd^{3+}; τ_m, the mean residence time of water molecules; and τ_R, the rotational correlation time of water molecules) are the most structure-related parameters that influence the performance of r_1^{IS}. The maximized q value and optimized τ_m and τ_R are required to obtain high r_1^{IS}. The diffusion correlation time of water molecules (τ_D) is the only parameter that affects r_1^{OS}. The increased τ_D value will result in higher r_1^{OS}. Interestingly, by taking advantage of the inherent differences in porosity between $dSiO_2$ and $mSiO_2$ shells, altered q and τ_m could be expected. In addition, different silica shell thickness may influence τ_R and τ_D, which could potentially provide a chance to investigate the involved relaxivity mechanisms (Figure 2).[15] It was observed that the r_1 value of UCNP@$mSiO_2$ remained nearly unchanged at around 4.8 mM^{-1} s^{-1} when the $mSiO_2$ shell thickness was tuned in the range from 11.1 to 23.4 nm, indicating the minor role of inner-sphere mechanism since both τ_m and τ_R are dependent on $mSiO_2$ thickness. In sharp contrast, r_1 values of UCNP@$dSiO_2$ increased rapidly along with the increasing $dSiO_2$ shell thicknesses from 2.6 to 16.9 nm, which can be perfectly explained by outer-sphere mechanism because the increased $dSiO_2$ thickness will lead to restricted outer-sphere water diffusion in $dSiO_2$, finally resulting in increased r_1^{OS} relaxivity.

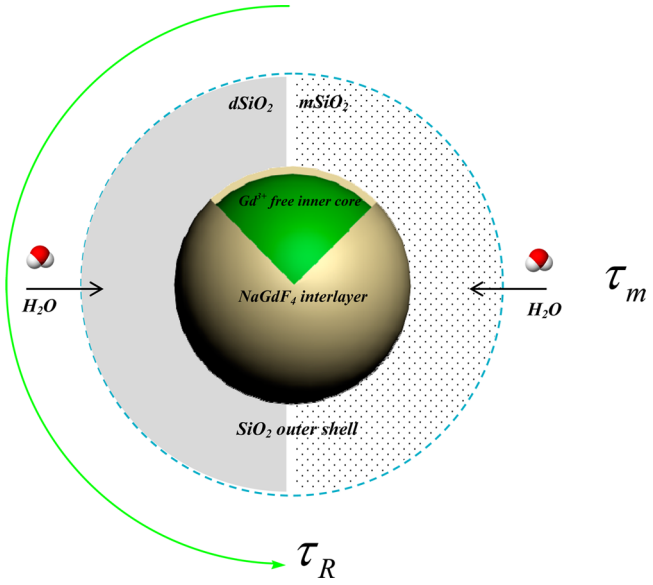

Figure 2. Well-designed silica coated Gd^{3+}-free $NaYF_4$:Yb/Er core@$NaGdF_4$ shell nanoprobes for investigating the MR relaxivity mechanism. Reproduced with permission from ref 15. Copyright 2013 John Wiley and Sons.

Under the guidance of the above mechanism investigation, the Gd^{3+} ions located on the particle surface were suggested to provide the main contributions to T_1-MR imaging.[17−19] Afterward, various highly efficient nanoprobes based on Gd-free core/$NaGdF_4$ shell-structured UCNPs have been investigated.[20] To optimize the r_1 value of Gd-UCNPs, decreasing the nanoparticles' size (smaller than 4 nm) can be another effective way to elevate the density of surface Gd^{3+} ions. We fabricated ultrasmall $NaGdF_4$ nanodots (~2 nm) with chelating diethylene triamine pentaacetic acid (DTPA) grafted outside to capture the potentially released Gd^{3+}, which exhibited a high r_1 value of 8.93 mM^{-1} s^{-1}.[21] Importantly, these nanodots demonstrate much stronger vascular signal than clinical Magnevist at the same dose; a considerable number of capillary vessels and atherosclerotic plaques can be clearly delineated with a high resolution. No doubt, the investigation of relaxivity mechanism will guide the design of other UCNP agents with unique and efficient UCL/T_1-MR bimodal imaging capability. As another MRI mode, T_2-weighted MRI can also achieve sensitive molecular imaging by using magnetic nanoparticles as probes through shortening the transverse relaxation time of surrounding water molecules.[22] It is worth mentioning that, among various lanthanide ions, a number of paramagnetic ions such as Dy^{3+}, Ho^{3+}, and Yb^{3+}, in addition to Gd^{3+}, are suggested to be promising T_2-MR probes.[23]

3.2. Multimodal Imaging

It is anticipated that multifunctional diagnosis probes can give more detailed information on tumors with both high resolution

DOI: 10.1021/acs.accounts.5b00078
Acc. Chem. Res. 2015, 48, 1797−1805

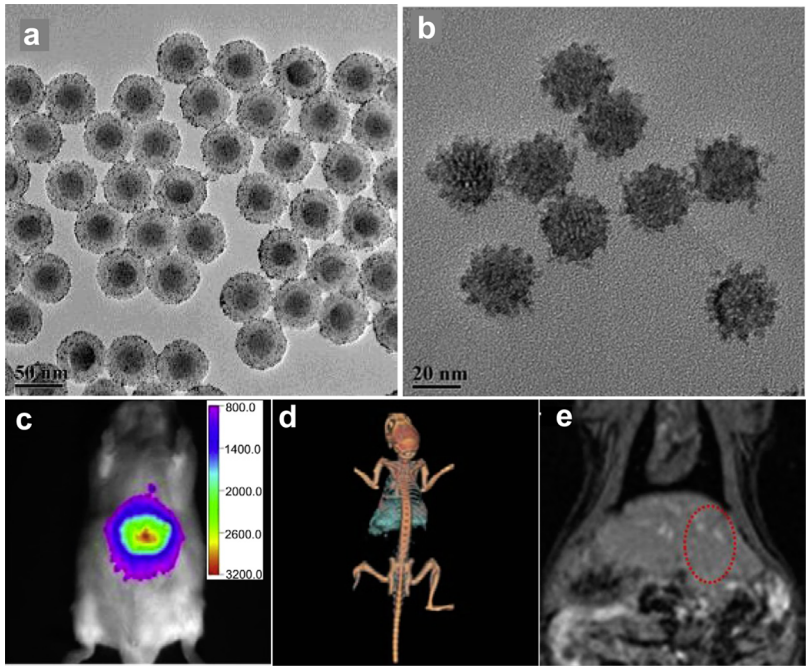

Figure 3. TEM images of Gd-UCNP@SiO_2−Au (a) and Gd-UCNP@TaO_x (b). Reproduced with permission from ref 26. Copyright 2012 Elsevier Ltd. (c−e) *In vivo* UCL/CT/T_1-MR imagings after intravenous injection of Gd-UCNP@TaO_x. Liver sites are marked with circles. Reproduced with permission from ref 27. Copyright 2012 Elsevier Ltd.

and sensitivity. However, how to design the high-performance trimode contrast agents without mutual interference is technically challenging. One way is to dope specific elements, which provide MR and X-ray computed tomography (CT) functions in UCNPs. Very recently, our group developed an efficient nanoprobe based on $NaYbF_4$:Ho for multimodal UCL/CT/MR imaging thanks to the simultaneous CT and T_2-MRI performance of both Yb and Ho.[24] As another solution, integration of differently functionalized components into one system is more appealing.[25] Due to the easy surface modification of silica, our group combined $NaYF_4$:Yb/Gd/Er/Tm with gold nanoparticles by electrostatic adsorption between electropositive UCNP@dSiO_2−NH_2 and negative gold nanoparticles (Figure 3a) for trimodal imaging: strong upconversion emissions for UCL imaging, Gd^{3+} for T_1-MRI, and gold nanoparticles for CT imaging.[26] Interestingly, the distance between the UCNP core and plasmonic gold nanoparticles at the surface can be well tuned by varying the thickness of the silica shell, which is very useful to manipulate plasmonic interaction for enhanced UCL emission. Practically, to prevent the UCL signal blocking by outer gold nanoparticles, recently a nanocomposite has been constructed by decorating Gd-UCNPs with radiopaque but luminescence-transparent tantalum oxide (TaO_x, $x \approx 1$) (Figure 3b) via a reverse micelle method.[27] After intravenous injection of the probes to the mice, high contrast UCL/CT/MR trimodal imagings *in vivo* (Figure 3c−e) could be achieved simultaneously, which will be greatly favorable for precisely determining the location of tumors. More attractively, the recent development of multifunctional UCNPs for hexamodal imaging (fluorescence/Cerenkov luminescence/UCL/photoacoustic/positron emission tomography/CT) further confirmed the potential of clinical application for UCNPs-based nanoprobes.[28]

3.3. Drug Delivery

Over the past decades, to minimize the systemic cytotoxicity of free drugs, various drug delivery systems have been constructed thanks to their great potential for further biomedical applications. Lin et al. developed a multifunctional nanocarrier composed of UCNP@mSiO_2 and pH/temperature-responsive P(NIPAm-*co*-MAA) polymer brush gatekeepers for simultaneous imaging and controlled chemotherapy.[29] At elevated temperature or lowered pH, the swelling of polymer located at the surface of mSiO_2 layer will trigger the release of DOX molecules encapsulated in the mesoporous shell.

Very recently, a NIR light-triggered anticancer drug release system was developed by integrating UCNP@mSiO_2 and photoresponsive azobenzene molecules into one system (Figure 4a).[30] Upon NIR light irradiation, the upconverted UV and visible luminescence from UCNPs can trigger the continuous back and forth wagging motions of the azobenzene molecules linked in the mesopore channels, which can thus propel the release of anticancer drugs. Soon afterward, a similar drug release system was also explored by Li's group by loading 7-amino-coumarin derivative-caged anticancer drug chlorambucil in the UCNP@hmSiO_2.[31] Under NIR exposure, the upconverted UV light from UCNPs can cleave the chemical bond of the aminocoumarin site, thus resulting in the release of the uncaged chlorambucil. Such nanocarriers possess the advantages of high drug-loading capacity and sensitivity to NIR light. These achievements provide a promising solution to the general problem of low tissue penetration of excitation light in traditional phototriggered drug release systems.

In clinical applications, the real time monitoring of anticancer drug release is very significant because insufficient or excess drug dosages are both undesirable. Xing and co-workers developed a NIR light-activated nanoplatform by combining an apoptosis-sensing peptide-conjugated UCNP@dSiO_2 with a photoactivatable platinum prodrug (Pt^{IV}).[32] After the activation

DOI: 10.1021/acs.accounts.5b00078
Acc. Chem. Res. 2015, 48, 1797−1805

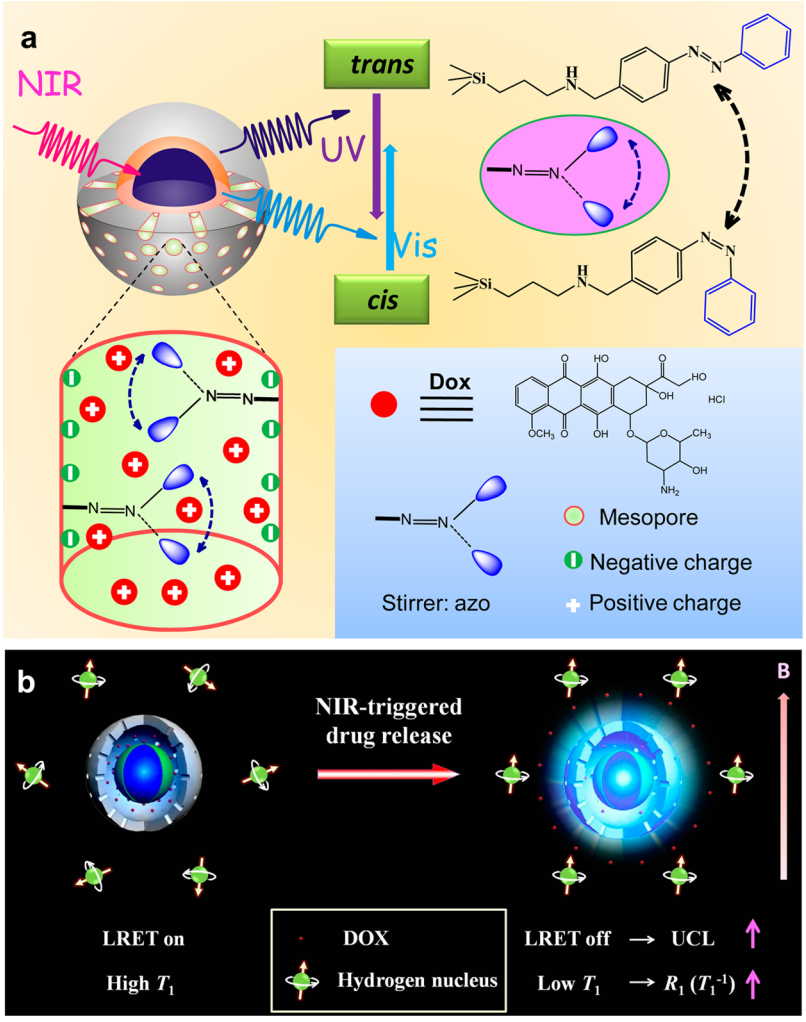

Figure 4. (a) The mechanism of NIR-triggered drug release. Reproduced with permission from ref 30. Copyright 2013 John Wiley and Sons. (b) Schematic illustration of monitoring drug release by MR imaging. Reproduced with permission from ref 13. Copyright 2014 John Wiley and Sons.

of Pt^{IV} complex by the upconverted emission from UCNPs, the generated caspases would effectively cleave the peptide conjugated on the silica surface, thus enabling the recovery of the quenched NIR fluorescence. As a result, the proposed nanotheranostic is capable of real-time imaging of the drug release. Our group further proposed a UCNP@hmSiO_2 nanocomposite and developed a novel concept of monitoring drug release *in vivo* using MR imaging.[13] As depicted in Figure 4b, along with the release of drug molecules, the amount of drugs in the hollow cavity will decrease, resulting in the increased probability of water molecules bonding to Gd^{3+} ions located in UCNPs core and consequently increased r_1 value of the designed nanosensors. Such a monitoring strategy is featured with the high resolution and tissue depth-independence of MRI, which can be possibly applied to online determining the drug concentrations *in vivo*.

3.4. PDT

Conventional PDT drugs are activated by visible light to generate reactive oxygen species (ROS) and singlet oxygen ($^1O_2$), which is able to kill the cancer cells.[33] However, they have been proven effective only in the treatment of superficial carcinoma, not deep cancer due to the poor penetration of visible light. Fortunately, the integration of UCNPs and PDT agents such as MC540 (merocyanine 540) and ZnPc (zinc phthalocyanine) can enable the PDT agent activation under NIR excitation by employing UCNPs as wavelength converters. For example, PDT agents can be chemically incorporated within UCNP@dSiO_2 via siloxane linkages.[34]

Typically, $NaYF_4$:Yb/Er UCNPs produce a green emission along with a red emission under NIR irradiation. In the above-mentioned systems, only a single band of upconverted emission was absorbed by PDT agents. To make use of other emission, Zhang's group developed a dual-photosensitizer approach, in which MC540 and ZnPc photosensitizers were loaded into $NaYF_4$:Yb/Er@mSiO_2 simultaneously (denoted as UCNs-ZnPc-MC540) (Figure 5a).[35] Such dual photosensitizers can be activated by both upconverted green and red emissions under a single NIR excitation. Compared with single photosensitizers, UCNs-ZnPc-MC540 demonstrated promoted generation of singlet oxygen and higher antitumor effect (Figure 5b).

Despite the extensive efforts in developing NIR-induced PDT, deep-located tumors remain mostly unaccessible. In addition, antitumor efficacy will be drastically decreased due to the remarkable oxygen consumption during continuing PDT. To address these issues, our group developed an X-ray-activated PDT strategy to treat deep tumors with diminished oxygen dependence using a Ce^{III}-doped $LiYF_4$@dSiO_2@ZnO

DOI: 10.1021/acs.accounts.5b00078
Acc. Chem. Res. 2015, 48, 1797−1805

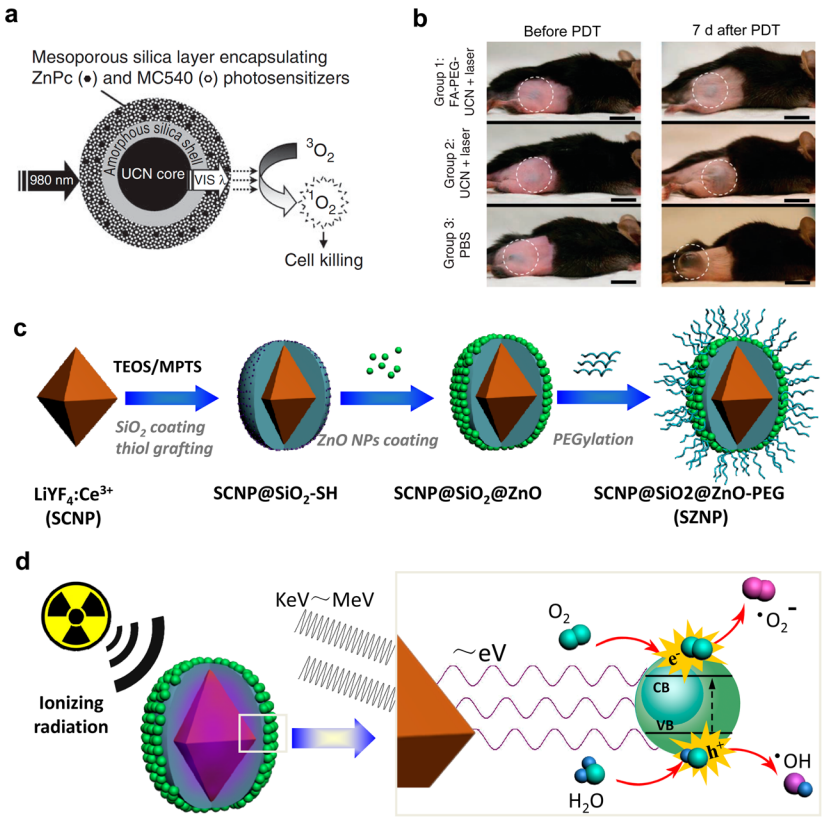

Figure 5. (a) Schematics of UCNP@dSiO$_2$@mSiO$_2$ coloaded with ZnPc and MC540 photosensitizers for PDT. (b) Representative photos of mice intravenously injected with FA-PEG-UCNs, unmodified UCNs or PBS. Scale bars, 10 mm. Reproduced with permission from ref 35. Copyright 2012 Nature Publishing Group. (c) Schematic illustration of the synthetic route to monodisperse SZNPs. (d) The mechanism of ionizing radiation-induced PDT. Reproduced with permission from ref 36. Copyright 2015 John Wiley and Sons.

structure (Figure 5c).[36] In brief, under X-ray radiation, UV light emitted from octahedral Ce^{3+}-doped $LiYF_4$ scintillating nanoparticle (SCNP) matches well with the bandgap of ZnO decorated on the surface of SCNP@dSiO$_2$, resulting in the formation of an electron−hole (e^-−h^+) pair. Notably, the reaction between h^+ and the absorbed water instead of oxygen can generate highly reactive hydroxyl radicals ($^{\bullet}OH$) (Figure 5d). Such a process essentially minimizes the oxygen tension dependency of ROS generation.

3.5. Synergetic Therapy

Recently, our group demonstrated that higher X-ray doses could be concentrated at the tumor regions containing the constitutive heavy elements due to their large X-ray photon capture cross-section and strong Compton scattering effect during radiotherapy.[37] As a result, a large amount of photoelectrons and Auger electrons can be concentrated in the regions of interest. Some specific anticancer drugs containing high-Z elements, such as cisplatin (CDDP) containing Pt, can be used as radiosensitizers, which will lead to simultaneous chemotherapy and radiotherapy by loading CDDP into theranostics. For example, CDDP loaded UCNP@hmSiO$_2$ nanotheranostics were designed to achieve optimized therapeutic efficacy via synergetic chemo- and radiotherapy, giving rise to much enhanced antitumor efficacy with reduced dosages of both chemodrug and X-ray.[38] In addition, because most anticancer drugs must reach the cell nucleus where they interact with DNA to stop cell growth,[39] our group further constructed a sub-50 nm UCNP@mSiO$_2$ nanotheranostic system to directly deliver radiosensitizing drug Mitomycin C into the nucleus. The results indicate that the substantially enhanced synergetic chemo- and radiotherapy can lead to efficient cancer treatment as well as circumvention of multidrug resistance *in vitro* and *in vivo*.[40]

Although the high-Z metal ion-sensitized radiotherapy can generate increased local radiation doses on deep-seated tumors, such an enhanced radiotherapy is not able to thoroughly kill radiotherapy-insensitive S-phase cells. Fortunately, these radioresistant cells are very sensitive to thermotherapy; therefore the combination of radiotherapy and photothermal ablation will offset the above disadvantage. Very recently, our group constructed multifunctional core/satellite nanotheranostics by decorating the surface of UCNP@dSiO$_2$ with ultrasmall CuS nanoparticles (Figure 6).[41] The UCNP inner core served as not only radiation dose-enhancer due to the existence of rare earth elements but also contrast agent for UCL/T_1-MR/CT trimodal

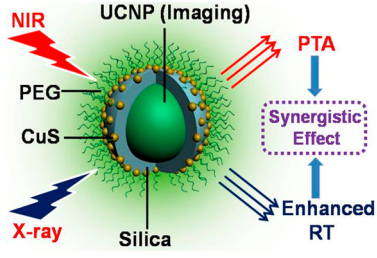

Figure 6. Schematic of a theranostics for the synergistic radiotherapy and photothermal ablation. Reproduced with permission from ref 41. Copyright 2013 American Chemical Society.

DOI: 10.1021/acs.accounts.5b00078
Acc. Chem. Res. 2015, 48, 1797−1805

imaging. In the meantime, CuS satellites were used as NIR-driven photothermal agents for efficient photothermal ablation. Such a combination showed much higher antitumor efficacy than the expected sum of two individual treatments.

It is widely known that regrowth of tumors due to the quick self-repair of DNA is a common drawback of current therapies. Fortunately, cytotoxic $^1O_2$ generated by PDT may be more effective in destroying cancer cells. Our group constructed a multifunctional UCNP@hmSiO$_2$ nanocomposite coloaded with hematoporphyrin and docetaxel.[42] Hematoporphyrin serving as photosensitizer was covalently grafted inside the silica shell while docetaxel applied as chemodrug was encapsulated into the inner cavity. Interestingly, both hematoporphyrin and docetaxel can be used as radiosensitizers. Hematoporphyrin has been reported to promote the generation of ROS under X-ray irradiation;[43] meanwhile, docetaxel-treated cells will remain in the G2−M phase of the cell cycle, by which cells become highly sensitive to radiotherapy.[44] Such an integration of chemotherapy/radiotherapy/PDT will enable synergetic therapeutic effect among different modes, thus leading to remarkably enhanced anticancer therapeutic effects.

Another possible factor that induces regrowth of tumors is the existence of hypoxic areas in tumors. Interestingly, a tunable ratiometric oxygen sensor was developed for the quantitative measurement of hypoxic level, which is important to guide the subsequent treatments of hypoxic tumors.[45] [Ru(dpp)$_3$]$^{2+}$Cl$_2$, whose maximum absorbance perfectly overlaps with the emission of UCNPs, was chosen as the indicator for sensing oxygen level. As shown in Figure 7, the efficient combination of

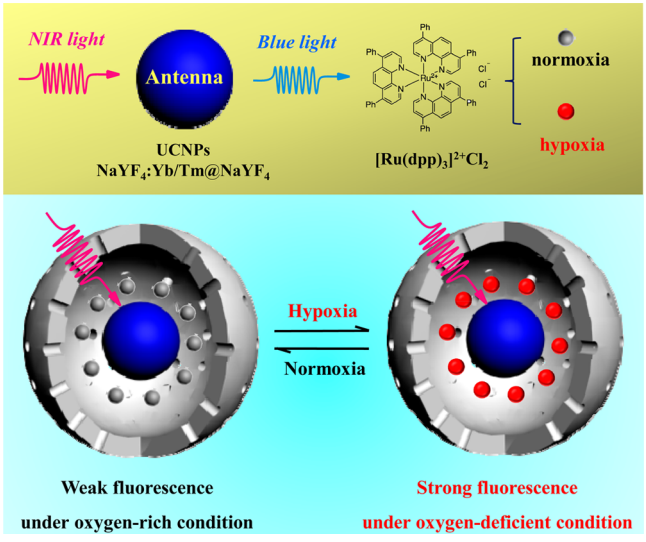

Figure 7. Schematic illustration of the nanosensor structure and its sensing to oxygen by detecting the change in luminescence emission intensity. Reproduced with permission from ref 45. Copyright 2014 American Chemical Society.

UCNPs and [Ru(dpp)$_3$]$^{2+}$Cl$_2$ into one system can be achieved by encapsulating [Ru(dpp)$_3$]$^{2+}$Cl$_2$ into the hollow cavity of UCNP@hmSiO$_2$. In particular, such a hollow cavity is especially beneficial to the energy transfer between UCNPs (donors) and [Ru(dpp)$_3$]$^{2+}$Cl$_2$ (acceptors) within 10 nm. More importantly, the local oxygen concentrations in the nanosensors will be significantly higher than those in outside solution due to adsorption of oxygen molecules into mesopores. As a result, it is possible to detect low concentrations of oxygen with high sensitivity. To treat hypoxic tumors more efficiently, a theranostic based on UCNP@hmSiO$_2$ has been constructed,[46] in which the UCNP core serves as radiation dose amplifier, while the bioreductive prodrug tirapazamine loaded in the cavity can be used as a hypoxia-selective cytotoxin to mitigate the oxygen dependence of radiotherapy. This theranostic shows effectively suppressed activities of hypoxic cells, thus resulting in substantial inhibition of hypoxia−reoxygenation and the subsequent cancer cell replication that often occurs after a single radiotherapy.

4. CONCLUSIONS AND PROSPECTS

Combining the unique properties of both UCNP core and silica shell, the UCNP@SiO$_2$ multifunctional nanocomposites can serve as effective agents for theranostic applications. However, there is still large space for enhancing the quantum yield of UCNPs. Currently, the core/shell structure is widely used to increase quantum efficiency.[47] To further elevate the quantum yield, new materials and synthetic strategies should be developed, especially aiming at synthesizing ultrasmall-sized UCNPs (within 10 nm) with high luminescent efficiency. Meanwhile, more effort should be made to rationally design smart theranostics that enable highly effective therapy under remote control and to establish relationships between imaging results and therapeutic efficacy, which will offer possibilities of monitoring the therapeutic outcome in real time. All these efforts may make personalized theranostics possible.

Overall, the development of UCNP@SiO$_2$-based theranostics for biomedical applications will continue to be an active and important research focus. Further intensive research on UCNP@SiO$_2$ will no doubt bring exciting and encouraging achievements to the chemistry and biomedicine communities by contributing new discoveries and overcoming challenges. Interdisciplinary collaborations are critically needed to further optimize the performance of UCNP@SiO$_2$-based theranostics and enable their successful application in the clinic.

AUTHOR INFORMATION

Corresponding Authors

*E-mail: wbbu@mail.sic.ac.cn (W.B.).
*E-mail: jlshi@mail.sic.ac.cn (J.S.).

Notes

The authors declare no competing financial interest.

Biographies

Jia-Nan Liu received his Ph.D. degree at Shanghai Institute of Ceramics, Chinese Academy of Sciences (SICCAS). He is now an assistant professor at SICCAS. His research is focused on the design, synthesis, and nanobiomedical applications of multifunctional UCNPs.

Wen-Bo Bu received his Ph.D. degree at Nanjing University of Technology. He is a full professor at SICCAS since 2008. He has published about 50 peer-reviewed research papers in *J. Am. Chem. Soc.*, *Angew. Chem.*, and *Adv. Mater.*, among others. His current research interests include the design and synthesis of multifunctional rare-earth based nanomaterials for future cancer imaging and therapeutic applications.

Jian-Lin Shi received his Ph.D. degree at SICCAS. He is now a full professor of SICCAS. His research areas include synthesis of multifunctional UCNPs, mSiO$_2$, and their biomedical applications. He has published over 300 scientific papers, which have been cited

DOI: 10.1021/acs.accounts.5b00078
Acc. Chem. Res. 2015, 48, 1797−1805

more than 11000 times by other scientists with an h-index of 58 (2014).

■ ACKNOWLEDGMENTS

This work was supported by the National Natural Science Foundation of China (Grant Nos. 51372260, 51132009, and 51402338), Youth Innovation Promotion Association CAS, and the Shanghai Yangfan Program (Grant No. 14YF1406400).

■ REFERENCES

(1) Haase, M.; Schäfer, H. Upconverting Nanoparticles. *Angew. Chem., Int. Ed.* **2011**, *50*, 5808−5829.
(2) Zhou, J.; Liu, Z.; Li, F. Upconversion Nanophosphors for Small-Animal Imaging. *Chem. Soc. Rev.* **2012**, *41*, 1323−1349.
(3) Park, Y. I.; Lee, K. T.; Suh, Y. D.; Hyeon, T. Upconverting Nanoparticles: A Versatile Platform for Wide-Field Two-Photon Microscopy and Multi-Modal In Vivo Imaging. *Chem. Soc. Rev.* **2015**, *44*, 1302−1317.
(4) Chen, G.; Qiu, H.; Prasad, P. N.; Chen, X. Upconversion Nanoparticles: Design, Nanochemistry, and Applications in Theranostics. *Chem. Rev.* **2014**, *114*, 5161−5214.
(5) Gai, S.; Li, C.; Yang, P.; Lin, J. Recent Progress in Rare Earth Micro/Nanocrystals: Soft Chemical Synthesis, Luminescent Properties, and Biomedical Applications. *Chem. Rev.* **2014**, *114*, 2343−2389.
(6) Muhr, V.; Wilhelm, S.; Hirsch, T.; Wolfbeis, O. S. Upconversion Nanoparticles: From Hydrophobic to Hydrophilic Surfaces. *Acc. Chem. Res.* **2014**, *47*, 3481−3493.
(7) Arriagada, F. J.; Osseo-Asare, K. Synthesis of Nanosize Silica in a Nonionic Water-in-Oil Microemulsion: Effects of the Water/Surfactant Molar Ratio and Ammonia Concentration. *J. Colloid Interface Sci.* **1999**, *211*, 210−220.
(8) Stöber, W.; Fink, A.; Bohn, E. Controlled Growth of Monodisperse Silica Spheres in the Micron Size Range. *J. Colloid Interface Sci.* **1968**, *26*, 62−69.
(9) Li, Z. Q.; Zhang, Y. Monodisperse Silica-coated Polyvinylpyrrolidone/$NaYF_4$ Nanocrystals with Multicolor Upconversion Fluorescence Emission. *Angew. Chem., Int. Ed.* **2006**, *45*, 7732−7735.
(10) Liu, J.; Bu, W.; Zhang, S.; Chen, F.; Xing, H.; Pan, L.; Zhou, L.; Peng, W.; Shi, J. Controlled Synthesis of Uniform and Monodisperse Upconversion Core/Mesoporous Silica Shell Nanocomposites for Bimodal Imaging. *Chem.—Eur. J.* **2012**, *18*, 2335−2341.
(11) Qian, H. S.; Guo, H. C.; Ho, P. C. L.; Mahendran, R.; Zhang, Y. Mesoporous-Silica-Coated Up-Conversion Fluorescent Nanoparticles for Photodynamic Therapy. *Small* **2009**, *5*, 2285−2290.
(12) Liu, B.; Li, C.; Yang, D.; Hou, Z.; Ma, P.; Cheng, Z.; Lian, H.; Huang, S.; Lin, J. Upconversion-Luminescent Core/Mesoporous-Silica-Shell-Structured β-$NaYF_4$:Yb^{3+},Er^{3+}@SiO_2@mSiO_2 Composite Nanospheres: Fabrication and Drug-Storage/Release Properties. *Eur. J. Inorg. Chem.* **2014**, *2014*, 1906−1913.
(13) Liu, J.; Bu, J.; Bu, W.; Zhang, S.; Pan, L.; Fan, W.; Chen, F.; Zhou, L.; Peng, W.; Zhao, K.; Du, J.; Shi, J. Real-Time In Vivo Quantitative Monitoring of Drug Release by Dual-Mode Magnetic Resonance and Upconverted Luminescence Imaging. *Angew. Chem., Int. Ed.* **2014**, *53*, 4551−4555.
(14) Kumar, R.; Nyk, M.; Ohulchanskyy, T. Y.; Flask, C. A.; Prasad, P. N. Combined Optical and MR Bioimaging Using Rare Earth Ion Doped $NaYF_4$ Nanocrystals. *Adv. Funct. Mater.* **2009**, *19*, 853−859.
(15) Chen, F.; Bu, W.; Zhang, S.; Liu, J.; Fan, W.; Zhou, L.; Peng, W.; Shi, J. Gd^{3+}-Ion-Doped Upconversion Nanoprobes: Relaxivity Mechanism Probing and Sensitivity Optimization. *Adv. Funct. Mater.* **2013**, *23*, 298−307.
(16) Werner, E. J.; Datta, A.; Jocher, C. J.; Raymond, K. N. High-Relaxivity MRI Contrast Agents: Where Coordination Chemistry Meets Medical Imaging. *Angew. Chem., Int. Ed.* **2008**, *47*, 8568−8580.
(17) Chen, F.; Bu, W.; Zhang, S.; Liu, X.; Liu, J.; Xing, H.; Xiao, Q.; Zhou, L.; Peng, W.; Wang, L.; Shi, J. Positive and Negative Lattice Shielding Effects Co-existing in Gd (III) Ion Doped Bifunctional Upconversion Nanoprobes. *Adv. Funct. Mater.* **2011**, *21*, 4285−4294.
(18) Chen, G.; Ohulchanskyy, T. Y.; Law, W. C.; Agren, H.; Prasad, P. N. Monodisperse $NaYbF_4$:Tm^{3+}/$NaGdF_4$ Core/Shell Nanocrystals with Near-infrared to Near-infrared Upconversion Photoluminescence and Magnetic Resonance Properties. *Nanoscale* **2011**, *3*, 2003−2008.
(19) Johnson, N. J. J.; Oakden, W.; Stanisz, G. J.; Prosser, R. S.; van Veggel, F. Size-Tunable, Ultrasmall $NaGdF_4$ Nanoparticles: Insights into Their T_1 MRI Contrast Enhancement. *Chem. Mater.* **2011**, *23*, 3714−3722.
(20) Ni, D.; Zhang, J.; Bu, W.; Xing, H.; Han, F.; Xiao, Q.; Yao, Z.; Chen, F.; He, Q.; Liu, J.; Zhang, S.; Fan, W.; Zhou, L.; Peng, W.; Shi, J. Dual-Targeting Upconversion Nanoprobes across the Blood-Brain Barrier for Magnetic Resonance/Fluorescence Imaging of Intracranial Glioblastoma. *ACS Nano* **2014**, *8*, 1231−1242.
(21) Xing, H.; Zhang, S.; Bu, W.; Zheng, X.; Wang, L.; Xiao, Q.; Ni, D.; Zhang, J.; Zhou, L.; Peng, W.; Zhao, K.; Hua, Y.; Shi, J. Ultrasmall $NaGdF_4$ Nanodots for Efficient MR Angiography and Atherosclerotic Plaque Imaging. *Adv. Mater.* **2014**, *26*, 3867−3872.
(22) Lee, J.-H.; Huh, Y.-M.; Jun, Y.-w.; Seo, J.-w.; Jang, J.-t.; Song, H.-T.; Kim, S.; Cho, E.-J.; Yoon, H.-G.; Suh, J.-S.; Cheon, J. Artificially Engineered Magnetic Nanoparticles for Ultra-sensitive Molecular Imaging. *Nat. Med.* **2007**, *13*, 95−99.
(23) Das, G. K.; Zhang, Y.; D'Silva, L.; Padmanabhan, P.; Heng, B. C.; Chye Loo, J. S.; Selvan, S. T.; Bhakoo, K. K.; Yang Tan, T. T. Single-Phase Dy_2O_3:Tb^{3+} Nanocrystals as Dual-Modal Contrast Agent for High Field Magnetic Resonance and Optical Imaging. *Chem. Mater.* **2011**, *23*, 2439−2446.
(24) Ni, D.; Bu, W.; Zhang, S.; Zheng, X.; Li, M.; Xing, H.; Xiao, Q.; Liu, Y.; Hua, Y.; Zhou, L.; Peng, W.; Zhao, K.; Shi, J. Single Ho^{3+}-Doped Upconversion Nanoparticles for High-Performance T_2-Weighted Brain Tumor Diagnosis and MR/UCL/CT Multimodal Imaging. *Adv. Funct. Mater.* **2014**, *24*, 6613−6620.
(25) Cheon, J.; Lee, J. H. Synergistically Integrated Nanoparticles as Multimodal Probes for Nanobiotechnology. *Acc. Chem. Res.* **2008**, *41*, 1630−1640.
(26) Xing, H.; Bu, W.; Zhang, S.; Zheng, X.; Li, M.; Chen, F.; He, Q.; Zhou, L.; Peng, W.; Hua, Y.; Shi, J. Multifunctional Nanoprobes for Upconversion Fluorescence, MR and CT Trimodal Imaging. *Biomaterials* **2012**, *33*, 1079−1089.
(27) Xiao, Q.; Bu, W.; Ren, Q.; Zhang, S.; Xing, H.; Chen, F.; Li, M.; Zheng, X.; Hua, Y.; Zhou, L.; Peng, W.; Qu, H.; Wang, Z.; Zhao, K.; Shi, J. Radiopaque Fluorescence-transparent TaO_x Decorated Upconversion Nanophosphors for In Vivo CT/MR/UCL Trimodal Imaging. *Biomaterials* **2012**, *33*, 7530−7539.
(28) Rieffel, J.; Chen, F.; Kim, J.; Chen, G.; Shao, W.; Shao, S.; Chitgupi, U.; Hernandez, R.; Graves, S. A.; Nickles, R. J.; Prasad, P. N.; Kim, C.; Cai, W.; Lovell, J. F. Hexamodal Imaging with Porphyrin-Phospholipid-Coated Upconversion Nanoparticles. *Adv. Mater.* **2015**, *27*, 1785−1790.
(29) Zhang, X.; Yang, P.; Dai, Y.; Ma, P. a.; Li, X.; Cheng, Z.; Hou, Z.; Kang, X.; Li, C.; Lin, J. Multifunctional Up-Converting Nanocomposites with Smart Polymer Brushes Gated Mesopores for Cell Imaging and Thermo/pH Dual-Responsive Drug Controlled Release. *Adv. Funct. Mater.* **2013**, *23*, 4067−4078.
(30) Liu, J.; Bu, W.; Pan, L.; Shi, J. NIR-Triggered Anticancer Drug Delivery by Upconverting Nanoparticles with Integrated Azobenzene-Modified Mesoporous Silica. *Angew. Chem., Int. Ed.* **2013**, *52*, 4375−4379.
(31) Zhao, L.; Peng, J.; Huang, Q.; Li, C.; Chen, M.; Sun, Y.; Lin, Q.; Zhu, L.; Li, F. Near-Infrared Photoregulated Drug Release in Living Tumor Tissue via Yolk-Shell Upconversion Nanocages. *Adv. Funct. Mater.* **2014**, *24*, 363−371.
(32) Min, Y.; Li, J.; Liu, F.; Yeow, E. K. L.; Xing, B. Near-Infrared Light-Mediated Photoactivation of a Platinum Antitumor Prodrug and Simultaneous Cellular Apoptosis Imaging by Upconversion-Luminescent Nanoparticles. *Angew. Chem., Int. Ed.* **2014**, *53*, 1012−1016.
(33) Celli, J. P.; Spring, B. Q.; Rizvi, I.; Evans, C. L.; Samkoe, K. S.; Verma, S.; Pogue, B. W.; Hasan, T. Imaging and Photodynamic Therapy: Mechanisms, Monitoring, and Optimization. *Chem. Rev.* **2010**, *110*, 2795−2838.

DOI: 10.1021/acs.accounts.5b00078
Acc. Chem. Res. 2015, 48, 1797−1805

(34) Chen, F.; Zhang, S.; Bu, W.; Chen, Y.; Xiao, Q.; Liu, J.; Xing, H.; Zhou, L.; Peng, W.; Shi, J. A Uniform Sub-50 nm-Sized Magnetic/Upconversion Fluorescent Bimodal Imaging Agent Capable of Generating Singlet Oxygen by Using a 980 nm Laser. *Chem.—Eur. J.* **2012**, *18*, 7082−7090.
(35) Idris, N. M.; Gnanasammandhan, M. K.; Zhang, J.; Ho, P. C.; Mahendran, R.; Zhang, Y. In Vivo Photodynamic Therapy Using Upconversion Nanoparticles as Remote-controlled Nanotransducers. *Nat. Med.* **2012**, *18*, 1580−1585.
(36) Zhang, C.; Zhao, K.; Bu, W.; Ni, D.; Liu, Y.; Feng, J.; Shi, J. Marriage of Scintillator and Semiconductor for Synchronous Radiotherapy and Deep Photodynamic Therapy with Diminished Oxygen Dependence. *Angew. Chem., Int. Ed.* **2015**, *54*, 1770−1774.
(37) Xing, H.; Zheng, X.; Ren, Q.; Bu, W.; Ge, W.; Xiao, Q.; Zhang, S.; Wei, C.; Qu, H.; Wang, Z.; Hua, Y.; Zhou, L.; Peng, W.; Zhao, K.; Shi, J. Computed Tomography Imaging-guided Radiotherapy by Targeting Upconversion Nanocubes with Significant Imaging and Radiosensitization Enhancements. *Sci. Rep.* **2013**, *3*, No. 1751.
(38) Fan, W.; Shen, B.; Bu, W.; Chen, F.; Zhao, K.; Zhang, S.; Zhou, L.; Peng, W.; Xiao, Q.; Xing, H.; Liu, J.; Ni, D.; He, Q.; Shi, J. Rattle-Structured Multifunctional Nanotheranostics for Synergetic Chemo-/Radiotherapy and Simultaneous Magnetic/Luminescent Dual-Mode Imaging. *J. Am. Chem. Soc.* **2013**, *135*, 6494−6503.
(39) Pan, L.; He, Q.; Liu, J.; Chen, Y.; Ma, M.; Zhang, L.; Shi, J. Nuclear-Targeted Drug Delivery of TAT Peptide-Conjugated Monodisperse Mesoporous Silica Nanoparticles. *J. Am. Chem. Soc.* **2012**, *134*, 5722−5725.
(40) Fan, W.; Shen, B.; Bu, W.; Zheng, X.; He, Q.; Cui, Z.; Zhao, K.; Zhang, S.; Shi, J. Design of An Intelligent Sub-50 nm Nuclear-targeting Nanotheranostic System for Imaging Guided Intranuclear Radiosensitization. *Chem. Sci.* **2015**, *6*, 1747−1753.
(41) Xiao, Q.; Zheng, X.; Bu, W.; Ge, W.; Zhang, S.; Chen, F.; Xing, H.; Ren, Q.; Fan, W.; Zhao, K.; Hua, Y.; Shi, J. A Core/Satellite Multifunctional Nanotheranostic for in Vivo Imaging and Tumor Eradication by Radiation/Photothermal Synergistic Therapy. *J. Am. Chem. Soc.* **2013**, *135*, 13041−13048.
(42) Fan, W.; Shen, B.; Bu, W.; Chen, F.; He, Q.; Zhao, K.; Zhang, S.; Zhou, L.; Peng, W.; Xiao, Q.; Ni, D.; Liu, J.; Shi, J. A Smart Upconversion-based Mesoporous Silica Nanotheranostic System for Synergetic Chemo-/Radio-/Photodynamic Therapy and Simultaneous MR/UCL Imaging. *Biomaterials* **2014**, *35*, 8992−9002.
(43) Takahashi, J.; Misawa, M. Characterization of Reactive Oxygen Species Generated by Protoporphyrin IX under X-ray Irradiation. *Radiat. Phys. Chem.* **2009**, *78*, 889−898.
(44) Seiwert, T. Y.; Salama, J. K.; Vokes, E. E. The Concurrent Chemoradiation Paradigm-General Principles. *Nat. Clin. Pract. Oncol.* **2007**, *4*, 86−100.
(45) Liu, J.; Liu, Y.; Bu, W.; Bu, J.; Sun, Y.; Du, J.; Shi, J. Ultrasensitive Nanosensors Based on Upconversion Nanoparticles for Selective Hypoxia Imaging in Vivo upon Near-Infrared Excitation. *J. Am. Chem. Soc.* **2014**, *136*, 9701−9709.
(46) Liu, Y.; Liu, Y.; Bu, W.; Xiao, Q.; Sun, Y.; Zhao, K.; Fan, W.; Liu, J.; Shi, J. Radiation-/Hypoxia-induced Solid Tumor Metastasis and Regrowth Inhibited by Hypoxia-Specific Upconversion Nanoradiosensitizer. *Biomaterials* **2015**, *49*, 1−8.
(47) Han, S.; Deng, R.; Xie, X.; Liu, X. Enhancing Luminescence in Lanthanide-Doped Upconversion Nanoparticles. *Angew. Chem., Int. Ed.* **2014**, *53*, 11702−11715.

DOI: 10.1021/acs.accounts.5b00078
Acc. Chem. Res. 2015, 48, 1797−1805